Journal of Solid State Chemistry 181 (2008) 1367–1376

Contents lists available at ScienceDirect

Journal of Solid State Chemistry

journal homepage: www.elsevier.com/locate/jssc

Crystal structures of lazulite-type oxidephosphates $Ti^{III}Ti_3^{IV}O_3(PO_4)_3$ and $M_4^{III}Ti_{27}^{IV}O_{24}(PO_4)_{24}$ (M^{III} = Ti, Cr, Fe)

M. Schöneborn [1], R. Glaum *, F. Reinauer

Institut für Anorganische Chemie, Universität Bonn, Gerhard-Domagk-Straße 1, D-53121 Bonn, Germany

ARTICLE INFO

Article history:
Received 12 November 2007
Accepted 27 February 2008
Available online 14 March 2008

Keywords:
Chemical vapour transport
Crystal growth
Lipscombite
Lazulite
Mixed-valent titanium
Second-sphere ligand-field effects

ABSTRACT

Single crystals of the oxidephosphates $Ti^{III}Ti_3^{IV}O_3(PO_4)_3$ (black), $Cr_4^{III}Ti_{27}^{IV}O_{24}(PO_4)_{24}$ (red-brown, transparent), and $Fe_4^{III}Ti_{27}^{IV}O_{24}(PO_4)_{24}$ (brown) with edge-lengths up to 0.3 mm were grown by chemical vapour transport. The crystal structures of these orthorhombic members (space group *F2dd*) of the lazulite/lipscombite structure family were refined from single-crystal data [$Ti^{III}Ti_3^{IV}O_3(PO_4)_3$: $Z=24$, $a=7.3261(9)$ Å, $b=22.166(5)$ Å, $c=39.239(8)$ Å, $R_1=0.029$, w$R_2=0.084$, 6055 independent reflections, 301 variables; $Cr_4^{III}Ti_{27}^{IV}O_{24}(PO_4)_{24}$: $Z=1$, $a=7.419(3)$ Å, $b=21.640(5)$ Å, $c=13.057(4)$ Å, $R_1=0.037$, w$R_2=0.097$, 1524 independent reflections, 111 variables; $Fe_4^{III}Ti_{27}^{IV}O_{24}(PO_4)_{24}$: $Z=1$, $a=7.4001(9)$ Å, $b=21.7503(2)$ Å, $c=12.775(3)$ Å, $R_1=0.049$, w$R_2=0.140$, 1240 independent reflections, 112 variables). For $Ti^{III}Ti^{IV}O_3(PO_4)_3$ a well-ordered structure built from dimers [$Ti_2^{III,IV}O_9$] and [$Ti_2^{IV,IV}O_9$] and phosphate tetrahedra is found. The metal sites in the crystal structures of $Cr_4Ti_{27}O_{24}(PO_4)_{24}$ and $Fe_4Ti_{27}O_{24}(PO_4)_{24}$, consisting of dimers [$M^{III}Ti^{IV}O_9$] and [$Ti_2^{IV,IV}O_9$], monomeric [$Ti^{IV}O_6$] octahedra, and phosphate tetrahedra, are heavily disordered. Site disorder, leading to partial occupancy of all octahedral voids of the parent lipscombite/lazulite structure, as well as splitting of the metal positions is observed. According to Guinier photographs $Ti_4^{III}Ti_{27}^{IV}O_{24}(PO_4)_{24}$ ($a=7.418(2)$ Å, $b=21.933(6)$ Å, $c=12.948(7)$ Å) is isotypic to the oxidephosphates $M_4^{III}Ti_{27}^{IV}O_{24}(PO_4)_{24}$ (M^{III}: Cr, Fe). The UV/vis spectrum of $Cr_4Ti_{27}O_{24}(PO_4)_{24}$ reveals a rather small ligand-field splitting $\Delta_o=14{,}370\,cm^{-1}$ and a very low nephelauxetic ratio $\beta=0.72$ for the chromophores [$Cr^{III}O_6$] within the dimers [$Cr^{III}Ti^{IV}O_9$].

1. Introduction

By investigation of the phase diagram $TiO_2/TiP_2O_7/TiPO_4$ (Fig. 1) three mixed-valent titanium(III,IV)-phosphates were discovered some years ago [2]. Subsequent studies revealed the approximate compositions $Ti_{31}O_{24}(PO_4)_{24}$, "$Ti_{95}O_{72}(PO_4)_{72}$", and $Ti_9O_4(PO_4)_8$ [3]. For $Ti_{31}O_{24}(PO_4)_{24}$ and "$Ti_{95}O_{72}(PO_4)_{72}$" isomorphic substitution of titanium(III) by chromium(III) was shown to be possible [3]. A close structural relationship of these oxidephosphates to titanium(IV)-oxidephosphate $Ti_5O_4(PO_4)_4$ [4] and the lazulite/lipscombite structure family [5,6] was concluded from their X-ray powder diffraction patterns and electron diffraction experiments [3]. The crystal structure of tetragonal β-$Fe_2O(PO_4)$ [7–9], which is the aristotype of this structure family, is represented in Fig. 2. Recently, we reported [10] a structural systematization of the lazulite/lipscombite structure family in terms of group–subgroup relations with particular emphasis on ternary and polynary titanium phosphates (e.g. [11–17]).

Despite of the aforementioned investigations the detailed crystal structures of $Ti_{31}O_{24}(PO_4)_{24}$, "$Ti_{95}O_{72}(PO_4)_{72}$" and their derivatives $M_4^{III}Ti_{27}O_{24}(PO_4)_{24}$ and $M^{III}Ti_3^{IV}O_3(PO_4)_3$ (M^{III}: Cr, Fe) remained in the dark.

Only recently we have reported the crystal structure of $V^{III}V_3^{IV}O_3(PO_4)_3$ [18], for which the Guinier diagram indicated a close structural relationship to "$Ti_{95}O_{72}(PO_4)_{72}$" ($\equiv Ti_{96}O_{72}(PO_4)_{72} \equiv 24 \times Ti^{III}Ti_3^{IV}O_3(PO_4)_3$). The latter formula will be used throughout this paper. This result intensified our interest in the crystal structures of the mixed-valent titanium(III,IV)-phosphates, because the hitherto characterized anhydrous phosphates of vanadium(IV) and titanium(IV) do not show any structural similarities ($Ti_5O_4(PO_4)_4$ [2–4], TiP_2O_7 [19], $(VO)_2P_2O_7$ [20–22], $(VO)(PO_3)_2$ [23,24]) in contrast to the mixed-valent binary oxides M_nO_{2n-1} ("Magnéli phases", *M*: Ti, V; e.g. [25,26]).

In this contribution we report on crystal growth of the titanium phosphates $Ti^{III}Ti_3^{IV}O_3(PO_4)_3$, $Ti_4^{III}Ti_{27}^{IV}O_{24}(PO_4)_{24}$, and $M_4^{III}Ti_{27}O_{24}(PO_4)_{24}$ (M^{III}: Cr, Fe) by chemical vapour transport [27], on their structural characterization from single-crystal data, and on the unusual UV/vis spectrum of $Cr_4^{III}Ti_{27}^{IV}O_{24}(PO_4)_{24}$.

2. Experimental

2.1. Synthesis and crystallization

$TiPO_4$ as starting material was obtained by chemical vapour transport experiments [28]. TiP_2O_7 was prepared as described in

* Corresponding author. Fax: +0228 73 56 60.
E-mail address: rglaum@uni-bonn.de (R. Glaum).
[1] See Ref. [1].

0022-4596/$ - see front matter © 2008 Elsevier Inc. All rights reserved.
doi:10.1016/j.jssc.2008.02.039

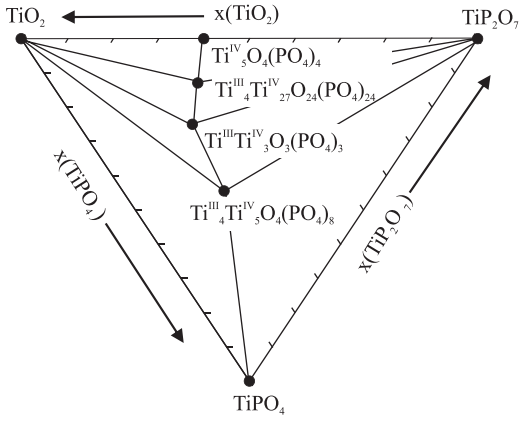

Fig. 1. Phase diagram $TiO_2/TiP_2O_7/TiPO_4$ at 1173 K [2,3].

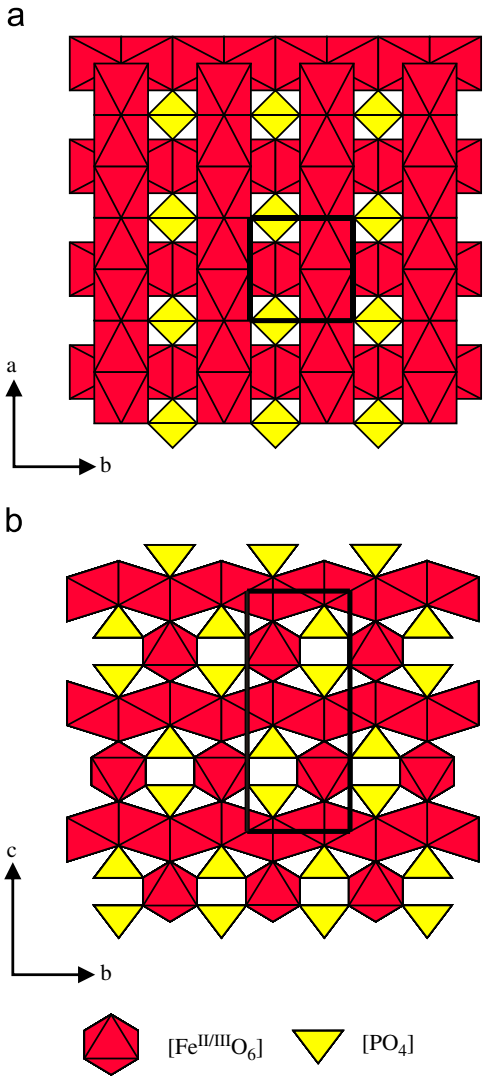

Fig. 2. Crystal Structure of tetragonal β-$Fe_2O(PO_4)$ [4–8]. Representation with $[Fe^{II,III}O_6]$ octahedra and $[PO_4]$ tetrahedra.

[29], anhydrous, amorphous $CrPO_4$ according to Brauer [30]. Microcrystalline $FePO_4$ was synthesized from iron(III) nitrate and stoichiometric amounts of H_3PO_4. Both educts were mixed in water, the solution was evaporated to dryness and the residue eventually heated at 1073 K in air for 24 h. Other reactants were at least of p. a. grade. Their phase composition was checked by Guinier photographs.

Microcrystalline powders of $M^{III}_4Ti_{27}O_{24}(PO_4)_{24}$ (M = Ti, Cr, Fe) and $Ti^{III}Ti^{IV}_3O_3(PO_4)_3$ were obtained by isothermal heating of stochiometric amounts of TiP_2O_7, TiO_2, and MPO_4 (M = Ti, Cr, Fe) according to

$$4\ MPO_{4,s} + 10\ TiP_2O_{7,s} + 17\ TiO_{2,s} = M^{III}_4Ti^{IV}_{27}O_{24}(PO_4)_{24,s}\ (M = \mathrm{Ti},\ \mathrm{Cr},\ \mathrm{Fe}) \quad (1)$$

$$TiPO_{4,s} + TiP_2O_{7,s} + 2\ TiO_{2,s} = Ti^{III}Ti^{IV}_3O_3(PO_4)_{3,s} \quad (2)$$

Starting materials were weighed into an agate mortar, ground together thoroughly and soaked at 1273 K in sealed silica ampoules for 3 days. According to *IP*-Guinier photographs single-phase products were thus obtained.

The oxidephosphates were crystallized by chemical vapour transport experiments [27,28] in sealed silica tubes (l∼12 cm, d∼1.5 cm, V∼21 cm^3). These tubes were placed in the temperature gradient of electrically heated two-zone furnaces. In all transport experiments stoichiometric mixtures (according to Eqs. (1) and (2) of MPO_4 (M = Ti, Cr, Fe), TiP_2O_7 and TiO_2 were used as starting materials.

Single crystals of $Cr^{III}_4Ti_{27}O_{24}(PO_4)_{24}$ (Fig. 3a) were grown using a mixture of $TiCl_4$ and PCl_3 (from *in situ* reaction of 2 mg TiP and 55 mg $PtCl_2$) as transporting agents (1273→1173 K, 14 days). About 15 mg of transparent, red-brown, tabular crystals with edge-lengths up to 0.2 mm were obtained at the sink side.

Crystallization of $Fe^{III}_4Ti_{27}O_{24}(PO_4)_{24}$ was achieved in transport experiments using as transport agent Cl_2 from *in situ* thermal decomposition of $PtCl_2$ (1273→1173 K, 14 days). Thus obtained crystals were brown and of irregular isometric shape with edge-lengths up to 0.3 mm. The yield of $Fe_4Ti_{27}O_{24}(PO_4)_{24}$ at the sink side was about 20 mg (Fig. 3b). The wall of the silica ampoule was heavily corroded in these experiments.

Crystals of $Ti^{III}Ti^{IV}_3O_3(PO_4)_3$ grown according to [2,3], using stochiometric amounts of the starting materials (Eq. (2)) and mixtures of 274 mg I_2 and 21.6 mg Ti (n(I):n(Ti) = 1.08:0.451) as transport agent showed heavy twinning and intergrowth and were not suitable for X-ray single-crystal diffraction experiments [3]. However, a transport experiment aiming at the formation of "$Ti^{III}_4Ti^{IV}_5O_4(PO_4)_8$", another, yet structurally not characterized titanium(III,IV)-phosphate, yielded the desired single crystals of $Ti^{III}Ti^{IV}_3O_3(PO_4)_3$ (Fig. 3c) with sufficient quality for data collection. Thus, single-crystal structure determination and refinement became eventually possible. In this transport experiment, 60 mg (0.42 mmol) $TiPO_4$, 46.59 mg (0.21 mmol) TiP_2O_7, and 25.16 mg (0.315 mmol) TiO_2 were used as starting materials together with 150 mg (0.59 mmol) I_2 as transporting agent. The ampoule was placed in a temperature gradient 1323→1223 K for 14 days. At the sink side about 40 mg of black crystals of $Ti^{III}Ti^{IV}_3O_3(PO_4)_3$ with average edge-lengths of 0.2 mm and a few (about 3 mg) green crystals of $TiPO_4$ were obtained.

For identification, examination of purity of the powder samples and for determination of lattice parameters Guinier photographs were taken using the image plate technique [31,32]. Details on this procedure have already been reported [33]. The lattice parameters were determined using the programme SOS [34].

The *UV/vis absorption* spectrum (Fig. 4) of a transparent red-brown $Cr_4Ti_{27}O_{24}(PO_4)_{24}$ crystal was measured at ambient temperature using a strongly modified CARY 17 microcrystal spectralphotometer (Spectra Services, ANU Canberra; for details see [35,36]). The incident light beam was perpendicular to the (001) face, with polarization along the perpendicular directions

Fig. 3. Crystals of $Cr_4^{III}Ti_{27}^{IV}O_{24}(PO_4)_{24}$, $Fe_4^{III}Ti_{27}^{IV}O_{24}(PO_4)_{24}$, and $Ti^{III}Ti_3^{IV}O_3(PO_4)_3$ from CVT experiments.

[310] and [$\bar{3}$10]. In these directions the crystal showed no optical anisotropy. Two broad bands at $\tilde{\nu}_1 = 14,370\,cm^{-1}$ and $\tilde{\nu}_2 = 20,000\,cm^{-1}$ are assigned to the spin-allowed transitions $^4A_{2g} \rightarrow {}^4T_{2g}(F)$ and $^4A_{2g} \rightarrow {}^4T_{1g}(F)$, respectively (all electronic states given for O_h symmetry). Dips in the region of the first absorption band at $\tilde{\nu}(^2E) = 14,025\,cm^{-1}$ and $\tilde{\nu}(^2T_{1g}) = 14,790\,cm^{-1}$ are caused by Fano-antiresonance [37–39] between the ^2E_g and the $^2T_{2g}$ states, respectively, and the spin–orbit split terms of the $^4T_{2g}$ state. The energy of the $^4A_{2g} \rightarrow {}^4T_{2g}(F)$ transition corresponds exactly to Δ_o. Spectroscopic data for $Cr_4Ti_{27}O_{24}(PO_4)_{24}$, $Cr_2(SO_4)_3$, and $Cr(PO_3)_3$ (*C-type*) are summarized in Table 1 for comparison.

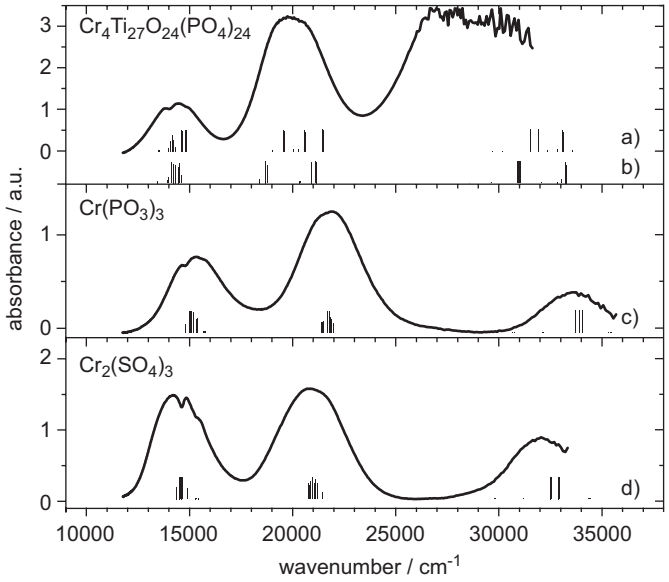

Fig. 4. UV/vis spectra of $Cr_4^{III}Ti_{27}^{IV}O_{24}(PO_4)_{24}$, $Cr(PO_3)_3$ and $Cr_2(SO_4)_3$. Ticks at the bottom of each spectrum represent calculated transition energies (see text for details). The length of a tick is related to the quartet character of the corresponding excited state.

Table 1
Evaluation of the electronic absorption spectra of $Cr_4^{III}Ti_{27}O_{24}(PO_4)_{24}$, $Cr(PO_3)_3$ (*C-type*), and $Cr_2(SO_4)_3$, all containing octahedral $[Cr^{III}O_6]$ chromophores

	$Cr_4^{III}Ti_{27}O_{24}(PO_4)_{24}$	$Cr_2(SO_4)_3$	$Cr(PO_3)_3$ (*C-type*)
$E(^4A_{2g} \rightarrow {}^4T_{2g}(F))/cm^{-1}$	14,370	14,600	15,380
$E(^4A_{2g} \rightarrow {}^2E_g(D))/cm^{-1}$	14,025	14,600	14,789
$E(^4A_{2g} \rightarrow {}^2T_{1g}(D))/cm^{-1}$	14,790	15,382	15,520
$E(^4A_{2g} \rightarrow {}^4T_{1g}(F))/cm^{-1}$	20,000	21,030	21,960
$E(^4A_{2g} \rightarrow {}^4T_{1g}(P))/cm^{-1}$	Not observed	32,000	33,580

2.2. X-ray single-crystal study

Intensity data for $Cr_4^{III}Ti_{27}^{IV}O_{24}(PO_4)_{24}$ and $Ti^{III}Ti_3^{IV}O_3(PO_4)_3$ were recorded on a κ-CCD diffractometer (Enraf-Nonius Inc.) and for $Fe_4^{III}Ti_{27}^{IV}O_{24}(PO_4)_{24}$ on an APEX SMART-CCD (Bruker AXS). The crystal structure determination of $Ti^{III}Ti_3^{IV}O_3(PO_4)_3$ by *Direct Methods* and its refinement allowing for anisotropic displacement parameters proceeded in a straightforward manner. After allowing for racemic twinnig the structure refined to reasonabel residuals. Crystallographic data as well as information on intensity data collection, structure determination, and refinement are summarized in Table 2. Atomic coordinates and interatomic distances are presented in Tables 3 and 4.

In contrast to $Ti^{III}Ti_3^{IV}O_3(PO_4)_3$, structure determination and refinement of $Cr_4^{III}Ti_{27}^{IV}O_{24}(PO_4)_{24}$ and $Fe_4^{III}Ti_{27}^{IV}O_{24}(PO_4)_{24}$ turned out to be much more complicated. For these quaternary oxidephosphates the X-ray single-crystal study revealed orthorhombic unit cells (a~7.4 Å, b~21.6 Å, c~13.0 Å) in agreement with an earlier investigation by electron diffraction [3]. Our X-ray work gave no hints on possible alternative unit cell choices. For $Cr_4^{III}Ti_{27}^{IV}O_{24}(PO_4)_{24}$, however, diffuse scattering along the c^* direction was observed. In the further course of the present investigation diffuse scattering was ignored. According to systematic extinctions and intensity distribution space groups *F2dd* and $C222_1$ were found as possible candidates (programmes WINGX [40] and XPREP [41]). For automated evaluation of systematic extinctions the maximum mean I/sigma(I) for absent reflections was set to 2.5. Interestingly, there is no direct symmetry relation between these two possible

Table 2
Crystallographic data, collection of intensity data, structure determination and refinement of the crystal structures of $Ti^{III}Ti^{IV}_3O_3(PO_4)_3$, $Cr^{III}_4Ti_{27}O_{24}(PO_4)_{24}$, and $Fe^{III}_4Ti_{27}O_{24}(PO_4)_{24}$

Chemical formula	$Cr^{III}_4Ti^{IV}_{27}O_{24}(PO_4)_{24}$	$Fe^{III}_4Ti^{IV}_{27}O_{24}(PO_4)_{24}$	$Ti^{III}Ti^{IV}_3O_3(PO_4)_3$
Formula weight [g/mol]	4164.58	4179.98	524.51
Crystal system	Orthorhombic	Orthorhombic	Orthorhombic
Space group	*F2dd* (no. 43)	*F2dd* (no. 43)	*F2dd* (no. 43)
Lattice parameters (from Guinier photographs)			
a [Å]	7.419(3)	7.4001(9)	7.3291(9)
b [Å]	21.640(5)	21.750(5)	22.166(5)
c [Å]	13.057(4)	12.775(3)	38.239(8)
Unit cell volume [Å^3]	2096.3(12)	2056.3(7)	6209.6(18)
Z	1	1	24
Absorp. coeff. [mm^{-1}]	3.543	3.789	3.539
Density (calculated)	3.299	3.376	3.366
Crystal colour	Red-brown	Brown	Black
Crystal shape	Square plate	Irregular-shaped isometric	Prismatic
Crystal size [mm^3]	0.192. 0.192. 0.04	0.15. 0.12. 0.11	0.2. 0.2. 0.2
F(000)	2010	2018	6072
Temperature [K]	293	293	293
Diffractometer	κ-CCD (Nonius)	APEX SMART-CCD	κ-CCD (Nonius)
Wavelength (Mo-Kα) 0.71073 Å. Graphite monochromator			
Theta range [°]	$3.30 \leqslant \theta \leqslant 30.32$	$3.32 \leqslant \theta \leqslant 28.72$	$3.00 \leqslant \theta \leqslant 33.61$
Absorption correction	Multiscans [57] after data reduction in WinGx [40]	Semi-empirical in XPREP [41]	Multiscans [57] after data reduction in WinGx [40]
Reflections collected	19876	3703	62487
Independent reflections	1524 [$R_{int} = 0.044$]	1240 [$R_{int} = 0.046$]	6055 [$R_{int} = 0.045$]
Index ranges	$-10 \leqslant h \leqslant 10$ $-30 \leqslant k \leqslant 30$ $-18 \leqslant l \leqslant 18$	$-9 \leqslant h \leqslant 9$ $-29 \leqslant k \leqslant 29$ $-17 \leqslant l \leqslant 11$	$-11 \leqslant h \leqslant 11$ $-34 \leqslant k \leqslant 34$ $-59 \leqslant l \leqslant 59$
Parameters	111	112	301
R indices [$I > 2\sigma(I)$]	$R_1 = 0.0369$ $wR_2 = 0.0966$	$R_1 = 0.0492$ $wR_2 = 0.1406$	$R_1 = 0.0294$ $wR_2 = 0.0840$
R indices (all data)	$R_1 = 0.0397$ $wR_2 = 0.0991$	$R_1 = 0.0550$ $wR_2 = 0.1456$	$R_1 = 0.0344$ $wR_2 = 0.0864$
Goodness-of-fit on F^2	1.074	1.107	1.149
BASF	0.49(10)	0.38(11)	0.66(2)
Weighting scheme	$A = 0.0468$, $B = 28.2912$	$A = 0.0056$, $B = 2.2109$	$A = 0.0546$, $B = 0$
Largest diff. peak and hole [e Å^{-3}]	1.460, −1.243	0.848, −0.798	1.198, −0.930

space groups. However, both are subgroups of $I4_1/amd$, the space group of the aristotype structure β-$Fe_2O(PO_4)$ [7–9]. Comparison of the unit cell volumes of $Cr^{III}_4Ti^{IV}_{27}O_{24}(PO_4)_{24}$ and $Fe^{III}_4Ti^{IV}_{27}O_{24}(PO_4)_{24}$ with that of β-$Fe_2O(PO_4)$ suggested $Z = 1$ for the polynary titanium oxidephosphates. Clearly, the distribution of 17 vacancies, four M^{3+}, and 27 Ti^{4+} over 48 octahedral voids, according to 24 $Fe_2O(PO_4) \equiv \square_{17}M^{III}_4Ti^{IV}_{27}O_{24}(PO_4)_{24}$, has to involve some sort of disorder.

In space group *F2dd* (no. 43) only, reasonable solutions for the chromium and iron compounds were found using *Direct Methods* (SHELXS [42] in programme suite WINGX [30]). In a different approach a starting model for the structure refinements in the candidate space group $C222_1$ (no. 20) was calculated by group–subgroup relations, based on the crystal structure of tetragonal β-$Fe_2O(PO_4)$. Even with this strategy in $C222_1$ refinement of a structure model was impossible for both oxidephosphates. Very high residuals and crystal chemical meaningless interatomic distances were thus obtained.

Eventually, both structures were refined in space group *F2dd*. Starting parameters for the metal and phosphorus atoms (*M*1, Ti2, P1, P2) and some oxygen atoms were revealed by *Direct Methods*. Subsequent Δ-Fourier syntheses allowed localisation of *M*3 and the missing oxygen atoms. Thus, in the structure model of $Fe_4Ti_{27}O_{24}(PO_4)_{24}$ significant electron density on all 48 octahedral voids, within the oxidephosphate network was found. These voids are related to metal positions *M*1, *M*2, and *M*3 (Table 7) on three general sites 16*b* in accordance with group–subgroup considerations. As a consequence of the chemical composition only 31 out of the 48 octahedral voids (3 × Wyckoff position 16*b* per unit cell) should be occupied and 17 holes per unit cell are expected. Thus, partial occupancy of at least some metal sites had to be considered. Calculations allowing free refinement of the site occupation factors for *M*1, *M*2, and *M*3 always led for *M*1 to an occupancy slightly below 1, while the sum s.o.f.(*M*2)+s.o.f.(*M*3) converged to values around 1.03.

In the next refinement step, mixed occupancy of the metal sites by Fe^{3+}/Ti^{4+} was accounted for. These calculations showed that site *M*1 only should host significant amounts of iron besides titanium. Eventually, we included a third type of disorder in the structure refinement of $Fe_4Ti_{27}O_{24}(PO_4)_{24}$, namely, the splitting of *M*1, *M*2, and *M*3 into *M*1A, *M*1B, *M*2A, *M*2B, *M*3A, and *M*3B (Tables 5 and 7). Such a disorder (“cation off-centering”) might be expected as a consequence of a cation or a vacancy on the octahedral void in the neighbourhood of *M*1, *M*2, and *M*3 (Fig. 9). To avoid high correlation factors among refined site occupancies and displacement parameters several constraints were introduced into the refinements. Eventually, the crystal structure of $Fe_4Ti_{27}O_{24}(PO_4)_{24}$ was refined assuming that the Fe^{3+} ions exclusively occupy metal position *M*1A (s.o.f.(*M*1A) = 4/16), that *M*1B hosts only Ti^{4+} (s.o.f.(*M*1B) = 11/16), and that the total occupancy of *M*2A, *M*2B, *M*3A, and *M*3B equals unity (SUMP instruction in SHELXL97 [43]). Phosphorus and oxygen atoms were refined with anisotropic displacement parameters.

The described structure model for $Fe_4Ti_{27}O_{24}(PO_4)_{24}$ was used as a starting point for the refinement of $Cr_4Ti_{27}O_{24}(PO_4)_{24}$. Immediately a very good fit was obtained. Racemic twinnig was allowed for in the final structure refinements of $Fe_4Ti_{27}O_{24}(PO_4)_{24}$ and $Cr_4Ti_{27}O_{24}(PO_4)_{24}$.

While crystals of the ternary titanium(III,IV)-oxidephosphate $Ti_4^{III}Ti_{27}^{IV}O_{24}(PO_4)_{24}$ are accessible by chemical vapour transport [2,3], no reasonable refinement of its crystal structure from single-crystal data could be accomplished so far [2,3]. Comparison of the powder diffraction pattern (Guinier photograph) of $Ti_4^{III}Ti_{27}^{IV}O_{24}(PO_4)_{24}$ with a simulation on the basis of the structure of $Cr_4^{III}Ti_{27}^{IV}O_{24}(PO_4)_{24}$ shows, however, acceptable agreement (Fig. 5).

For $Fe_4Ti_{27}O_{24}(PO_4)_{24}$ and $Cr_4Ti_{27}O_{24}(PO_4)_{24}$ information on crystal data, intensity measurement and structure refinement is summarized in Table 2. Final atomic coordinates, isotropic displacement parameters and interatomic distances are given in Tables 5–8. Supplementary material has been deposited with Fachinformationszentrum Karlsruhe, Abt. IDNT, D-76344 Eggenstein-Leopoldshafen (e-mail: crysdata@fiz-karlsruhe.de) and can be obtained by contacting FIZ [reference numbers: CSD-419242 for $Cr_4^{III}Ti_{27}^{IV}O_{24}(PO_4)_{24}$, CSD-419241 for $Fe_4^{III}Ti_{27}^{IV}O_{24}(PO_4)_{24}$, and CSD-419243 for $Ti^{III}Ti_3^{IV}O_3(PO_4)_3$.

Table 3
$Ti^{III}Ti_3^{IV}O_3(PO_4)_3$. Atomic coordinates and isotropic displacement parameters

Atom	Position	x	y	z	U_{eq} [Å^2][a]
Ti1	16*b*	0.3058(1)	0.7134(1)	0.4529(1)	0.0081(1)
Ti2	16*b*	0.2974(1)	0.7169(1)	0.7908(1)	0.0104(1)
Ti3	16*b*	0.3498(1)	0.7044(1)	0.1264(1)	0.0103(1)
Ti4	16*b*	0.3509(1)	0.6346(1)	0.2066(1)	0.0109(1)
Ti5	16*b*	0.3428(1)	0.6337(1)	0.5350(1)	0.0083(1)
Ti6	16*b*	0.3001(1)	0.0531(1)	0.1202(1)	0.0077(1)
P1	8*a*	0.6832(2)	3/4	3/4	0.0078(2)
P2	16*b*	0.7124(2)	0.5818(1)	0.9145(1)	0.0069(2)
P3	16*b*	0.2020(2)	0.7482(1)	0.9178(1)	0.0077(2)
P4	16*b*	0.1875(2)	0.4147(1)	0.9184(1)	0.0077(2)
P5	16*b*	0.7063(2)	0.5825(1)	0.2506(1)	0.0075(2)
O1	16*b*	0.2918(3)	0.7073(1)	0.5574(1)	0.0144(4)
O2	16*b*	0.2961(4)	0.7863(1)	0.2747(1)	0.0155(4)
O3	16*b*	0.3448(3)	0.7876(1)	0.6016(1)	0.0146(4)
O4	16*b*	0.8135(3)	0.3691(1)	0.5177(1)	0.0139(4)
O5	16*b*	0.3225(3)	0.1257(1)	0.2734(1)	0.0107(3)
O6	16*b*	0.2815(3)	0.1304(1)	0.6047(1)	0.0171(4)
O7	16*b*	0.3266(3)	0.5474(1)	0. 626(1)	0.0144(4)
O8	16*b*	0.3318(3)	0.5521(1)	0.7245(1)	0.0142(4)
O9	16*b*	0.3311(3)	0.4626(1)	0.6071(1)	0.0100(4)
O10	16*b*	0.8459(3)	0.7037(1)	0.1889(1)	0.0136(4)
O11	16*b*	0.8698(3)	0.7855(1)	0.9760(1)	0.0143(4)
O12	16*b*	0.8179(3)	0.7928(1)	0.6465(1)	0.0116(4)
O13	16*b*	0.8159(3)	0.3677(1)	0.1943(1)	0.0157(4)
O14	16*b*	0.8402(3)	0.3757(1)	0.0652(1)	0.0105(3)
O15	16*b*	0.8525(3)	0.3701(1)	0.8603(1)	0.0112(4)
O16	16*b*	0.8335(3)	0.5456(1)	0.6895(1)	0.0114(4)
O17	16*b*	0.8081(3)	0.5436(1)	0.0206(1)	0.0111(4)
O18	16*b*	0.8329(3)	0.4686(1)	0.6425(1)	0.0155(4)
O19	8*a*	0.4715(5)	1/2	0	0.0142(6)
O20	16*b*	0.2270(3)	0.7600(1)	0.0861(1)	0.0120(4)
O21	16*b*	0.6784(3)	0.9179(1)	0. 837(1)	0.0136(4)
O22	16*b*	0.7121(3)	0.9241(1)	0.4186(1)	0.0126(4)
O23	16*b*	0.6708(3)	0.9078(1)	0.7546(1)	0.0107(4)

[a] $U_{eq} = (1/3)\Sigma_i\Sigma_{jij}U_{ij}a_i^*a_j^*\boldsymbol{a}_i\cdot\boldsymbol{a}_j$.

3. Results and discussion

The mixed-valent titanium(III,IV)-oxidephosphates $Ti^{III}Ti_3^{IV}O_3(PO_4)_3$ (Fig. 6) and $Ti_4^{III}Ti_{27}O_{24}(PO_4)_{24}$ (Fig. 7), as well as the isotypic oxidephosphates $M_4^{III}Ti_{27}O_{24}(PO_4)_{24}$ (M = Cr, Fe), are

Table 5
Atomic coordinates and isotropic displacement parameters of $Cr_4Ti_{27}O_{24}(PO_4)_{24}$ [Å^2]

Atom	Position	x	y	z	S.o.f.	U_{eq} [Å^2][a]
Cr1	16*b*	0.2262(4)	0.7063(1)	0.8821(2)	4/16	0.0047(6)
Ti1	16*b*	0.2621(2)	0.7151(1)	0.8635(1)	11/16	0.0121(3)
Ti2A	16*b*	0.2264(7)	0.3675(2)	0.8717(4)	0.192(12)	0.0075(3)
Ti2B	16*b*	0.2176(3)	0.3651(1)	0.8932(1)	0.566(13)	0.0075(3)
Ti3A	16*b*	0.2160(40)	0.0372(13)	0.8790(20)	0.025(3)	0.0047(9)
Ti3B	16*b*	0.2634(6)	0.0533(2)	0.8594(3)	0.215(4)	0.0047(9)
P1	16*b*	0.6129(3)	0.3332(1)	0.0047(1)	1	0.0100(2)
P2	8*a*	0.6217(3)	0	0	1	0.0098(4)
O1	16*b*	0.4927(6)	0.7908(2)	0.1837(3)	1	0.0201(8)
O2	16*b*	0.4920(8)	0.1192(2)	0.1781(3)	1	0.0293(12)
O3	16*b*	0.4684(8)	0.4583(2)	0.1840(3)	1	0.0232(9)
O4	16*b*	−0.0123(6)	0.02945(2)	0.05736(3)	1	0.0212(8)
O5	16*b*	−0.0059(7)	0.06224(1)	0.05619(3)	1	0.0197(9)
O6	16*b*	0.0069(9)	0.9602(2)	0.5714(3)	1	0.0274(10)
O7	8*a*	0.0835(8)	0	0	1	0.0206(13)
O8	16*b*	0.3788(10)	0.5857(3)	0.2414(2)	1	0.0282(8)

[a] $U_{eq} = (1/3)\Sigma_i\Sigma_{jij}U_{ij}a_i^*a_j^*\boldsymbol{a}_i\cdot\boldsymbol{a}_j$.

Table 4
Interatomic distances for $Ti^{III}Ti_3^{IV}O_3(PO_4)_3$

[Ti1Ti4O$_9$]		[Ti2Ti5O$_9$]		[Ti3Ti6O$_9$]	
Ti1–O20	1.7024(19)	Ti2–O19	1.812(1)	Ti3–O21	1.821(2)
Ti1–O8	1.870(2)	Ti2–O7	1.848(3)	Ti3–O18	1.882(2)
Ti1–O11	1.885(2)	Ti2–O10	1.956(2)	Ti3–O6	1.905(2)
Ti1–O14	2.107(2)	Ti2–O17	2.074(2)	Ti3–O9	2.075(2)
Ti1–O16	2.108(2)	Ti2–O5	2.137(2)	Ti3–O12	2.117(2)
Ti1–O23	2.210(2)	Ti2–O22	2.183(2)	Ti3–20	2.168(2)
Ti4–O21	1.801(2)	Ti5–O23	1.703(2)	Ti6–O22	1.696(2)
Ti4–O4	1.874(2)	Ti5–O13	1.851(2)	Ti6–O3	1.882(2)
Ti4–O2	1.935(2)	Ti5–O1	1.880(2)	Ti6–O15	1.897(2)
Ti4–O14	2.093(2)	Ti5–O17	2.086(2)	Ti6–O9	2.080(2)
Ti4–O16	2.084(2)	Ti5–O5	2.039(2)	Ti6–O12	2.076(2)
Ti4–O23	2.197(2)	Ti5–O22	2.389(2)	Ti6–O20	2.320(2)
Ti1–Ti4	3.0690(7)	Ti2–Ti5	3.1140(7)	Ti3–Ti6	3.1014(8)

[P1O$_4$]		[P2O$_4$]		[P3O$_4$]		[P4O$_4$]		[P5O$_4$]	
O2	1.492(2)	O10	1.491(2)	O18	1.494(2)	O6	1.502(2)	O4	1.497(2)
O2	1.492(2)	O14	1.491(2)	O3	1.507(2)	O7	1.507(3)	O11	1.513(2)
O17	1.547(2)	O15	1.505(2)	O1	1.520(2)	O13	1.514(2)	O8	1.514(2)
O17	1.547(2)	O9	1.550(2)	O16	1.543(2)	O12	1.535(2)	O5	1.551(2)

Standard deviations in parentheses.

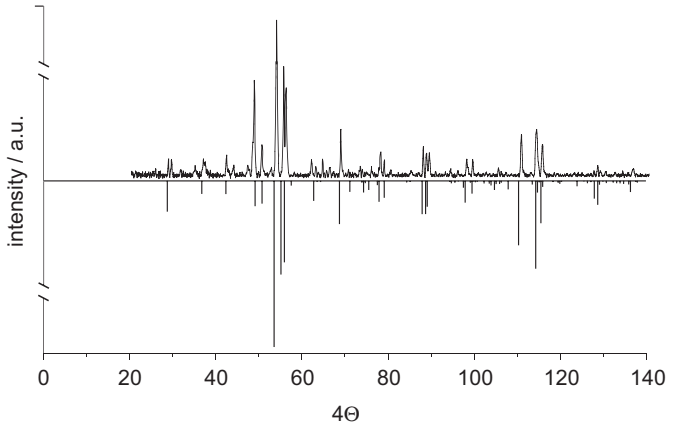

Fig. 5. Guinier-photograph (CuKα_1) of $Ti^{III}_4Ti^{IV}_{27}O_{24}(PO_4)_{24}$ and powder pattern simulated on the basis of the $Cr^{III}_4Ti^{IV}_{27}O_{24}(PO_4)_{24}$ structure model.

Table 6
$Cr_4Ti_{27}O_{24}(PO_4)_{24}$. Interatomic distances [Å] in polyhedra [$Cr^{III}O_6$], [$Ti^{IV}O_6$], and [PO_4]

[Cr1O$_6$]		[Ti1O$_6$]		[Ti2AO$_6$]	
Cr1–O8	1.841(5)	Ti1–O7	1.746(2)	Ti2A–O6	1.819(5)
Cr1–O1	1.934(5)	Ti1–O4	1.876(5)	Ti2A–O2	1.879(8)
Cr1–O5	1.937(4)	Ti1–O3	1.923(4)	Ti2A–O8	2.047(7)
Cr1–O3	1.970(4)	Ti1–O5	2.015(3)	Ti2A–O8	2.118(8)
Cr1–O4	2.025(5)	Ti1–O1	2.095(5)	Ti2A–O1	2.146(6)
Cr1–O7	2.122(4)	Ti1–O8	2.232(4)	Ti2A–O5	2.178(7)
Cr1–Ti3A	2.50(3)	Ti1–Ti3A	2.18(3)	Ti2A–Ti3B	2.119(9)
Cr1–Ti2A	2.670(6)	Ti1–Ti3B	2.690(5)	Ti2A–Ti3A	2.60(4)
Cr1–Ti2B	2.771(3)	Ti1–Ti2A	2.999(6)	Ti2A–Cr1	2.670(6)
Cr1–Ti3B	2.993(6)	Ti1–Ti2B	3.077(2)	Ti2A–Ti1	2.999(6)
[Ti2BO$_6$]		[Ti3AO$_6$]		[Ti3BO$_6$]	
Ti2B–O8	1.763(5)	Ti3A–O4	1.92(3)	Ti3B–O8	1.897(7)
Ti2B–O6	1.903(4)	Ti3A–O3	2.02(3)	Ti3B–O2	1.909(5)
Ti2B–O2	1.945(6)	Ti3A–O7	2.03(3)	Ti3B–O6	2.041(7)
Ti2B–O1	2.111(4)	Ti3A–O2	2.13(3)	Ti3B–O4	2.175(6)
Ti2B–O5	2.150(6)	Ti3A–O6	2.25(3)	Ti3B–O3	2.274(7)
Ti2B–O8	2.377(5)	Ti3A–O8	2.40(3)	Ti3B–O7	2.546(6)
Ti2B–Ti3B	2.022(5)	Ti3A–Ti1	2.18(3)	Ti3B–Ti2B	2.022(5)
Ti2B–Ti3A	2.53(3)	Ti3A–Ti2B	2.53(3)	Ti3B–Ti2A	2.119(9)
Ti2B–Cr1	2.771(3)	Ti3A–Cr1	2.50(3)	Ti3B–Ti1	2.690(5)
Ti2B–Ti1	3.077(2)	Ti3A–Ti2A	2.60(4)	Ti3B–Cr1	2.993(6)
[P1O$_4$]		[P2O$_4$]			
P1–O3	1.508(4)	P2–O6 (2x)	1.528(5)		
P1–O2	1.515(5)	P2–O1 (2x)	1.529(4)		
P1–O4	1.540(4)				
P1–O5	1.508(4)				

members of the lipscombite/lazulite structure family [4–7] as already assumed in earlier investigations [2–4]. Tetragonal β-$Fe_2O(PO_4)$, which is the aristotype of the whole family, crystallizes in space group $I4_1/amd$ ($a = 5.344(5)$ Å, $c = 12.460(8)$ Å, $Z = 4$) Its structure is built from chains of face-sharing octahedra [$Fe^{II/III}O_6$] along the [100] and [010] directions (Fig. 2). Each octahedron [$Fe^{II/III}O_6$] shares four vertices with [PO_4] tetrahedra. The remaining two vertices are occupied by oxide ions, which crosslink the chains. The oxide ions are coordinated by four iron atoms, while the oxygen atoms of phosphate groups are connected to two iron (and phosphorus; $c.n.(O_{phosphate}) = 3$) [5–9]. The unit cells of $Cr^{III}_4Ti^{IV}_{27}O_{24}(PO_4)_{24}$ and $Fe^{III}_4Ti^{IV}_{27}O_{24}(PO_4)_{24}$ are related to that of β-$Fe_2O(PO_4)$ by the transformation in Eq. (3). The transformation in Eq. (4) links the unit cells of $Ti^{III}Ti^{IV}_3O_3(PO_4)_3$ and β-$Fe_2O(PO_4)$:

$$(a,b,c)\begin{pmatrix}\bar{1} & 3 & 0\\ 1 & 3 & 0\\ 0 & 0 & \bar{1}\end{pmatrix} = (a',b',c'); \quad \det\begin{pmatrix}\bar{1} & 3 & 0\\ 1 & 3 & 0\\ 0 & 0 & \bar{1}\end{pmatrix} = 6 \tag{3}$$

$$(a,b,c)\begin{pmatrix}\bar{1} & 3 & 0\\ 1 & 3 & 0\\ 0 & 0 & \bar{3}\end{pmatrix} = (a',b',c'); \quad \det\begin{pmatrix}\bar{1} & 3 & 0\\ 1 & 3 & 0\\ 0 & 0 & \bar{3}\end{pmatrix} = 18 \tag{4}$$

In contrast to β-$Fe_2O(PO_4)$, where all octahedral voids are occupied, 2/6 of the voids in $Ti^{III}Ti^{IV}_3O_3(PO_4)_3$ ("$\square_2Ti^{III}Ti^{IV}_3O_3(PO_4)_3$"; "$\square$" denotes an octahedral void) and 17/48 in

Table 7
Atomic coordinates and isotropic displacement parameters of $Fe_4Ti_{27}O_{24}(PO_4)_{24}$ [Å^2]

Atom	Position	x	y	z	S.o.f.	U_{eq} [Å^2][a]
Fe1	16b	0.2229(6)	0.7057(2)	0.8775(3)	4/16	0.0098(10)
Ti1	16b	0.2632(3)	0.71570(8)	0.8652(1)	11/16	0.0133(5)
Ti2A	16b	0.2177(9)	0.3651(3)	0.8758(5)	0.228(3)	0.0029(4)
Ti2B	16b	0.2183(4)	0.3656(1)	0.8937(2)	0.480(5)	0.0029(4)
Ti3A	16b	0.247(4)	0.0383(14)	0.872(2)	0.059(6)	0.0095(13)
Ti3B	16b	0.2667(8)	0.0538(4)	0.8580(5)	0.23109	0.0095(13)
P1	16b	0.6134(3)	0.33377(9)	0.00516(7)	1	0.0100(4)
P2	8a	0.6216(3)	0	0	1	0.0076(5)
O1	16b	0.4922(9)	0.7911(2)	0.1833(4)	1	0.0179(12)
O2	16b	0.4919(11)	0.1196(2)	0.1766(5)	1	0.0272(16)
O3	16b	0.4708(11)	0.4584(2)	0.1853(5)	1	0.0244(15)
O4	16b	−0.0125(8)	0.2953(2)	0.5728(4)	1	0.0205(12)
O5	16b	−0.0035(10)	0.6227(2)	0.5616(4)	1	0.0211(15)
O6	16b	0.0090(12)	0.9606(2)	0.5715(5)	1	0.0257(15)
O7	8°	0.0837(13)	0	0	1	0.0243(19)
O8	16b	0.3792(15)	0.5844(3)	0.2412(3)	1	0.0303(13)

[a] $U_{eq} = (1/3)\Sigma_i\Sigma_j U_{ij} a_i^* a_j^* \boldsymbol{a}_i \cdot \boldsymbol{a}_j$.

Table 8
$Fe_4Ti_{27}O_{24}(PO_4)_{24}$. Interatomic distances [Å] in polyhedra [$Fe^{III}O_6$], [$Ti^{IV}O_6$], and [PO_4]

[Fe1O$_6$]		[Ti1O$_6$]		[Ti2AO$_6$]	
Fe1–O8	1.831(7)	Ti1–O7	1.731(4)	Ti2A–O6	1.813(8)
Fe1–O1	1.877(8)	Ti1–O4	1.855(7)	Ti2A–O2	1.830(10)
Fe1–O5	1.911(6)	Ti1–O3	1.905(5)	Ti2A–O8	1.940(0)
Fe1–O3	2.010(6)	Ti1–O5	2.045(5)	Ti2A–O1	2.176(8)
Fe1–O4	2.059(8)	Ti1–O1	2.104(7)	Ti2A–O8	2.207(10)
Fe1–O7	2.062(6)	Ti1–O8	2.182(6)	Ti2A–O5	2.239(10)
Fe1–Ti3A	2.71(3)	Ti1–Ti3A	2.35(3)	Ti2A–Ti3B	2.008(11)
Fe1–Ti2A	2.731(8)	Ti1–Ti3B	2.703(9)	Ti2A–Ti3A	2.34(4)
Fe1–Ti2B	2.733(5)	Ti1–Ti2B	3.085(3)	Ti2A–Fe1	2.731(8)
Fe1–Ti3B	3.051(9)	Ti1–Ti2A	3.096(7)	Ti2A–Ti1	3.096(7)
[Ti2BO$_6$]		[Ti3AO$_6$]		[Ti3BO$_6$]	
Ti2B–O8	1.749(7)	Ti3A–O4	1.93(3)	Ti3B–O8	1.834(11)
Ti2B–O6	1.921(6)	Ti3A–O6	2.07(3)	Ti3B–O2	1.891(8)
Ti2B–O2	1.928(8)	Ti3A–O2	2.12(3)	Ti3B–O6	2.032(9)
Ti2B–O1	2.099(6)	Ti3A–O7	2.20(3)	Ti3B–O4	2.212(10)
Ti2B–O5	2.151(8)	Ti3A–O3	2.17(3)	Ti3B–O3	2.274(10)
Ti2B–O8	2.360(8)	Ti3A–O8	2.18(3)	Ti3B–O7	2.548(10)
Ti2B–Ti3B	2.008(8)	Ti3A–Ti1	2.35(3)	Ti3B–Ti2B	2.008(8)
Ti2B–Ti3A	2.36(3)	Ti3A–Ti2A	2.34(4)	Ti3B–Ti2A	2.008(11)
Ti2B–Fe1	2.733(5)	Ti3A–Ti2B	2.36(4)	Ti3B–Ti1	2.703(9)
Ti2B–Ti1	3.085(3)	Ti3A–Fe1	2.71(3)	Ti3B–Fe1	3.051(9)
[P1O$_4$]		[P2O$_4$]			
P1–O3	1.506(6)	P2–O6 (2x)	1.504(6)		
P1–O2	1.508(7)	P2–O1 (2x)	1.524(6)		
P1–O4	1.521(6)				
P1–O5	1.540(6)				

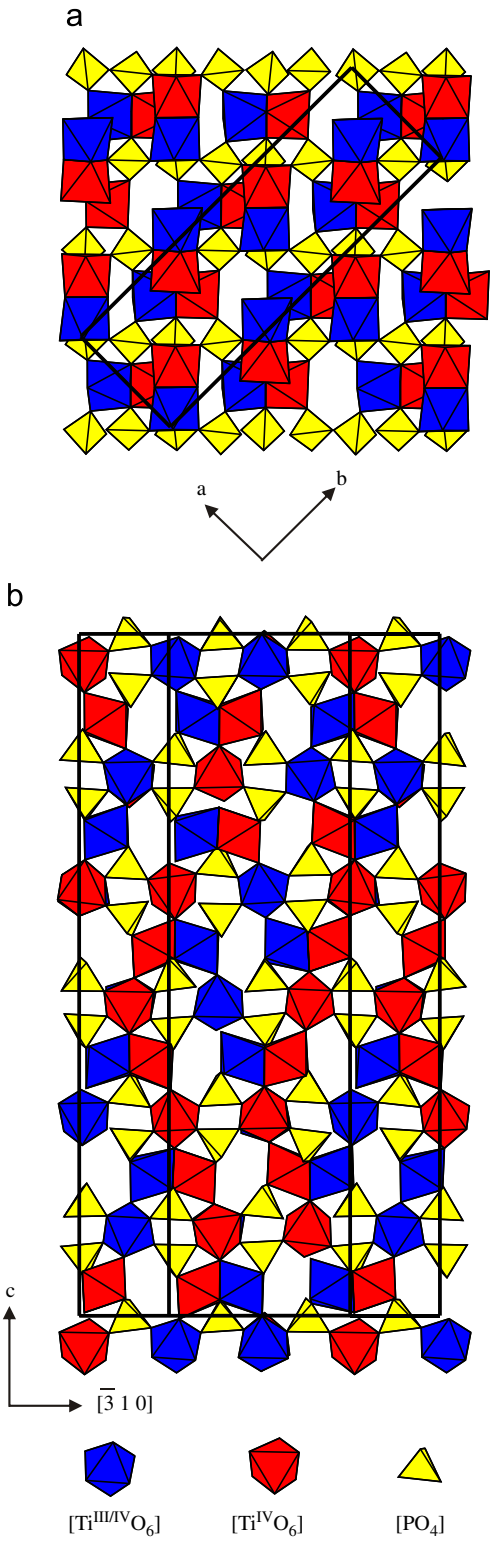

Fig. 6. $Ti^{III}Ti_3^{IV}O_3(PO_4)_3$. Projections along [001] and [310] of the crystal structure. For better clarity only slabs with thichnesses $c/6$ and $d_{(130)}$ are given.

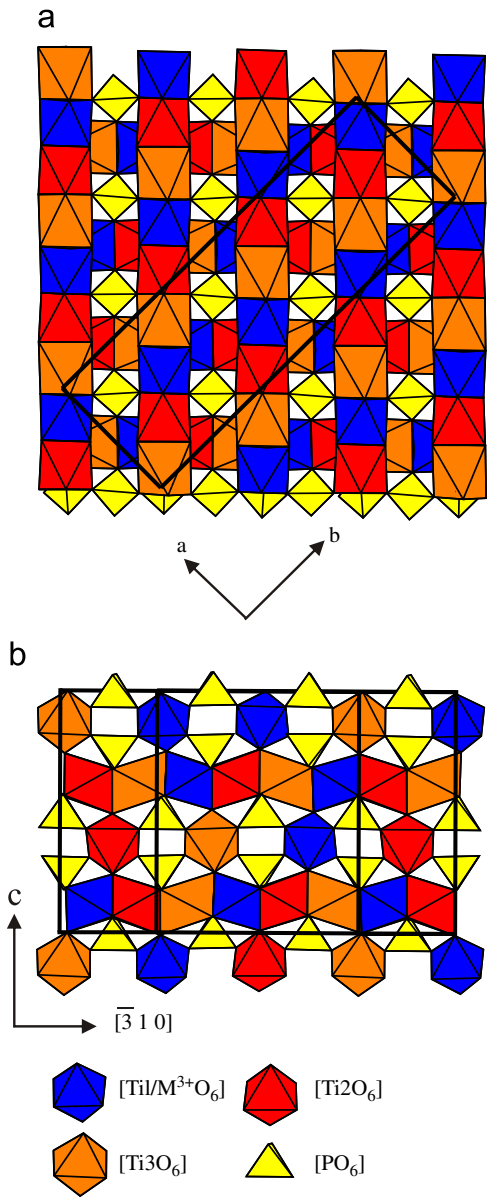

Fig. 7. $M_4^{III}Ti_{27}^{IV}O_{24}(PO_4)_{24}$ (M = Ti, Cr, Fe). Projections along [001] and [310] of the crystal structure. For better clarity only slabs with thicknesses $c/2$ and $d_{(130)}$ are given.

$M_4^{III}Ti_{27}O_{24}(PO_4)_{24}$ ("$\square_{17}M_4^{III}Ti_{27}^{IV}O_{24}(PO_4)_{24}$", M = Ti, Cr, Fe) are remaining vacant. For $Ti^{III}Ti_3^{IV}O_3(PO_4)_3$ a highly ordered structure is found with an occupancy sequence …, □, Ti, Ti, □, Ti, Ti, □, Ti, Ti, … for the octahedral voids. Thus, the main structural motif are double octahedra [Ti1Ti4O9], [Ti2Ti5O9], and [Ti3Ti6O9] (Fig. 8). Caused by electrostatic repulsion between adjacent titanium ions in the $[Ti_2O_9]$ dimers a radial distortion of the $[TiO_6]$ groups is found, leading to three longer distances d(Ti–O_b) to bridging oxygen atoms and to three shorter distances d(Ti–O_t) to terminal oxygen. For $Ti^{III}Ti_3^{IV}O_3(PO_4)_3$ no hints on disorder of the titanium atoms including the vacant octahedral sites were found. As one might conclude from variations in the distances d(Ti–O) within these dimers (Table 4) one titanium position (Ti1, Ti5, Ti6) is exclusively occupied by titanium(IV). Sites Ti4, Ti2, and Ti3 are more likely to contain 50% titanium(III) and 50% titanium(IV). This cation distribution is in contrast to that found for the isotypic vanadium(III,IV)-oxidephosphate $V^{III}V_3^{IV}O_3(PO_4)_3$ [18], in which four metal sites are exclusively occupied by vanadium(IV) and one by vanadium(III), showing typical distances $d(V^{IV}–O)$ and $d(V^{III}–O)$. The sixth vanadium site has an occupancy of 50% vanadium(III) and 50% vanadium(IV). However, this site is split, leading to two sites with distinctly different distances d(V–O). In space group $F2dd$ no ordered distribution of the 24 metal(III) and 72 metal(IV) cations per unit cell over the six independent metal sites (Wyckoff position 16b) is possible (Fig. 9).

For the lipscombite/lazulite structure family follows from simple charge-balance considerations the correlation between average charge of the cations (n) and the occupancy ($occu$) of the octahedral voids (Fig. 10.). Far less trivial is an answer to the question concerning the distribution pattern of cations over the available voids for a given composition. Full occupancy of the voids, probably with alternating cations M^{II} and M^{III}, is observed for oxidephosphates $M^{II,III}_2O(PO_4)$ ($n = 2.5+$, $occu = 1$, $M^{II,III}$: V/V, Fe/Fe, Ni/Cr). Increasing the average oxidation number to 3.33+ leads to an occupancy of 0.75. Oxidephosphates $M^{II}Ti^{IV}_2O_2(PO_4)_2$ (M^{II}: Fe, Co, Ni, Cu) [10,14–16] match these numbers and show a highly ordered arrangement of trimeric units $[O_3Ti^{IV}O_3M^{II}O_3Ti^{IV}O_3]$ separated by vacancies. Also for oxidephosphates $M^{III}M^{IV}_3O_3(PO_4)_3$ ($n = 3.75+$, $occu = 2/3$, $M^{III,IV}$: Ti/Ti, V/V [17], Cr/Ti [2]) and $Ti^{IV}_5O_4(PO_4)_4$ ($n = 4$, $occu = 5/8$; two types of dimers $[Ti^{IV}_2O_9]$ and one isolated octahedron $[Ti^{IV}O_6]$, separated by vacant sites [2–4]) well-ordered distributions of the cations over the voids are observed. In this context the apparently highly disordered arrangement of the cations in the oxidephosphates $\square_{17}M^{III}_4Ti^{IV}_{27}O_{24}(PO_4)_{24}$ ($M = Ti$, Cr, Fe; $n = 3.87+$, $occu = 0.646$) seems quite surprising. However, we believe that the site occupancy factors reported for $Cr^{III}_4Ti^{IV}_{27}O_{24}(PO_4)_{24}$ (Table 5) and $Fe^{III}_4Ti^{IV}_{27}O_{24}(PO_4)_{24}$ (Table 7) support the idea of at least some ordering of the cations. Neglecting the splitting of the sites, for $M2$ and $M3$ (both Wyckoff position 16b) a total occupancy of 1 is found from the refinements of the chromium and iron compound. This leaves for site $M1$ in both compounds, due to limitations by stoichiometry, s.o.f($M1$) = 15/16. For $Fe^{III}_4Ti^{IV}_{27}O_{24}(PO_4)_{24}$ the occupancy of the sites is visualized by Fig. 9. Assuming that a simultaneous occupancy of three consecutive octahedral voids is very unlikely due to electrostatic repulsion of the highly charged cations, one immediately arrives at a distribution of 4 dimers $[M^{III}Ti^{IV}O_9]$, 11 dimers $[Ti^{IV}_2O_9]$ and one isolated octahedron $[Ti^{IV}O_6]$ over the 48 voids of the unit cell. This is exactly the same distribution one might expect for a 1:1 combination of the structural motifs of $M^{III}Ti^{IV}_3O_3(PO_4)_3$ and $Ti^{IV}_5O_4(PO_4)_4$, the neighbouring phases to $M^{III}_4Ti^{IV}_{27}O_{24}(PO_4)_{24}$ (Fig. 10). Thus, even the observed cation disorder is in agreement with a very distinct composition of oxidephosphates $M^{III}_4Ti^{IV}_{27}O_{24}(PO_4)_{24}$. Clearly, the distribution of the metal cations over the three sites $M1$, $M2$, and $M3$ causes additional disorder with a splitting of the sites, due to electrostatic repulsion between cations in adjacent voids (Fig. 9). Of course, this splittings have to cause some relaxation of the surrounding lattice. We attribute slightly enlarged and more anisotropic displacement parameters for phosphorus and oxygen atoms in the refinements for $M^{III}_4Ti^{IV}_{27}O_{24}(PO_4)_{24}$ ($M = Cr$, Fe) to this effect.

The structural consequences (strict charge localization for the vanadium compound; partial delocalization for the titanium compound) found in the structures of $Ti^{III}Ti^{IV}_3O_3(PO_4)_3$ and $V^{III}V^{IV}_3O_3(PO_4)_3$ illustrate the higher crystal chemical similarity of the redox pair Ti^{III}/Ti^{IV} in contrast to V^{III}/V^{IV}. Concerning crystal chemical similarities and differences between anhydrous phosphates of titanium and vanadium it is quite notable that for these

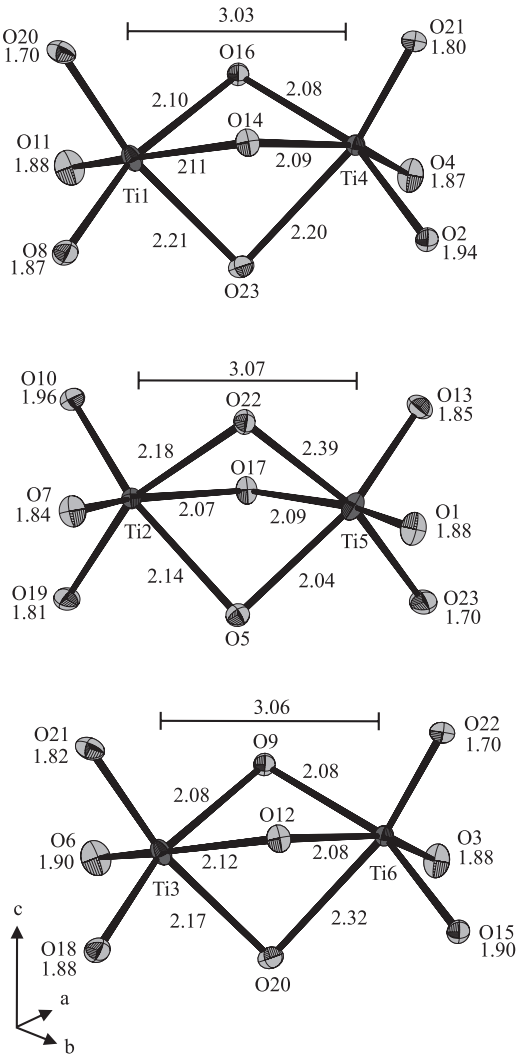

Fig. 8. ORTEP of the dimers $[Ti_2O_9]$ in $Ti^{III}Ti^{IV}_3O_3(PO_4)_3$. Ellipsoids given at the 50% probability level.

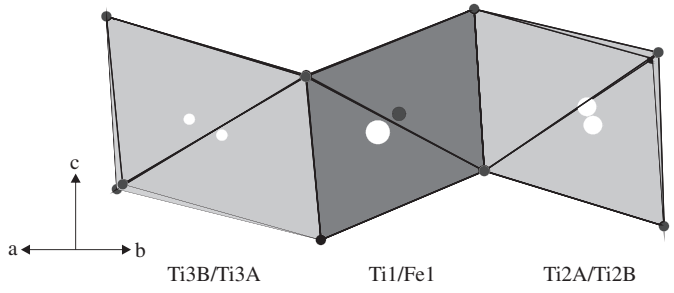

Fig. 9. Disorder of the cations Fe^{3+} and Ti^{4+} among sites $M1$A to $M3$B in $Fe^{III}_4Ti^{IV}_{27}O_{24}(PO_4)_{24}$. The size of the spheres visualizes the occupancy found for the various voids.

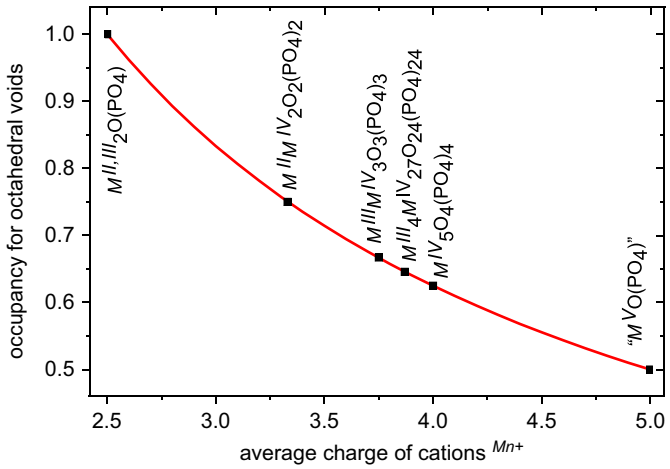

Fig. 10. Occupancy of octahedral voids with respect to the average charge of cations in lipscombite/lazulite-type oxidephosphates.

Table 9
AOM parametrization for the $[Cr^{III}O_6]$ chromophores in $Cr_4^{III}Ti_{27}O_{24}(PO_4)_{24}$, $Cr_2(SO_4)_3$, and $Cr(PO_3)_3$ (*C-type*)

	$Cr_4^{III}Ti_{27}O_{24}(PO_4)_{24}$		$Cr_2(SO_4)_3$	$Cr(PO_3)_3$
Chromophore	$[Cr^{III}Ti^{IV}O_9]$	$[Cr^{III}Ti_2^{IV}O_{12}]$	$[Cr^{III}O_6]$	$[Cr^{III}O_6]$
$d(Cr–O)_{min}$/Å	1.842	–	1.945	1.950
$e_{\sigma,max}(Cr–O)$/cm	8400	5100	7600	7900
$e_\pi(Cr–O)$	$e_{\pi,iso}(O_b) = 0\,cm^{-1}$ $e_{\pi,iso}(O_t) = 1/4e\sigma$	$e_{\pi,iso} = 0\,cm^{-1}$	$e_{\pi,iso} = 1/4e\sigma$	$e_{\pi,iso} = 1/4e\sigma$
$e_{\sigma,max}(Cr–Ti)$/cm	−500	−500(2x)	–	–
B/cm^{-1}	672	672	728	746
C/B	4.0	4.0	4.0	4.0
ζ/cm	198	198	215	220
β	0.72	0.72	0.78	0.80
TREE/cm	100	100	100	100

tetravalent cations not a single phosphate exists for both metals (titanium(IV): $Ti_5O_4(PO_4)_4$ [4], TiP_2O_7 [19], no silicophosphate; vanadium(IV): $(VO)_2P_2O_7$ [20–22], $VO(PO_3)_2$ [23,24], $(VO)Si(PO_4)_2$ [44]).

The UV/vis electronic absorption spectrum observed for $Cr_4^{III}Ti_{27}O_{24}(PO_4)_{24}$ (Fig. 4) reflects the particular bonding situation for the Cr^{3+} ions in this compound. In comparison to the more typical spectra observed for $Cr(PO_3)_3$ (*C-type* [45]) and $Cr_2(SO_4)_3$ several differences are obvious (Fig. 4; Table 1). These are a rather small ligand-field splitting $\Delta_o = 14{,}370\,cm^{-1}$, a low nephelauxetic ratio $\beta = B/B_{free\ ion} = 0.72$ and low-lying, strong charge-transfer transitions that obscure the *d*–*d* transition $^4A_{2g} \rightarrow {}^4T_{1g}(P)$.

Calculations (computer programme CAMMAG [46–48]) within the angular overlap model (AOM) [49–51] were carried out to get some insight into the bonding situation of the Cr^{3+} ions in the oxidephosphate, the sulphate and the metaphosphate. Details on this type of modelling were already reported in several publications (e.g. [10,52,53]). Despite the already discussed presence of dimers $[Cr^{III}Ti^{IV}O_9]$ in $Cr_4^{III}Ti_{27}O_{24}(PO_4)_{24}$ we included also modelling of the spectrum on the basis of a fictitious chromophore $[Cr^{III}Ti_2^{IV}O_{12}]$ (trimer of three face-sharing octahedra with Cr^{3+} in the central octahedron; geometric structure taken from the $[Ni^{II}Ti_2^{IV}O_{12}]$ chromophore in $NiTi_2O_2(PO_4)_2$ [10,14]). For $Cr(PO_3)_3$ (*C-type* [45]) and $Cr_2(SO_4)_3$ [54] the actual geometric structure of the chromophores $[Cr^{III}O_6]$ from the single-crystal structure refinements were taken. Table 9 summarizes the results of the best-fit calculations. In Fig. 4, the observed spectra are compared to the calculated transition energies. The calculations for the $[Cr^{III}Ti^{IV}O_9]$ chromophore in $Cr_4^{III}Ti_{27}O_{24}(PO_4)_{24}$ and the chromophores $[Cr^{III}O_6]$ in $Cr(PO_3)_3$ and $Cr_2(SO_4)_3$ match the observed transition energies nicely. For the sulphate and the metaphosphate very similar parameters were obtained, with only small differences in the interelectronic repulsion parameter and the ligand–metal σ-interaction. In contrast, the modeling for $Cr_4^{III}Ti_{27}O_{24}(PO_4)_{24}$ based on the $[Cr^{III}Ti^{IV}O_9]$ chromophore had to allow for a significantly reduced nephelauxetic ratio $\beta = B/B_{free\ ion} = 0.72$, for strongly modified ligand–metal π-interaction, and for a weak direct interaction between chromium and titanium. These findings are consistent with earlier work by Reinen [55] as well as from our group [10,52,53], were the importance of so-called second-sphere ligand-field effects [55,56] has already been pointed out. In the case of face-sharing between a chromphore $[MO_6]$ and an octahedron $[Ti^{IV}O_6]$ the highly charged d^0 cation pulls electron density from the neighbouring cation by σ- and π-interaction via the bridging oxygen atoms. Additionally, a weak direct metal–metal interaction leads to further reduction of the *d*-electron density at metal *M*. The AO modelling for $Cr_4^{III}Ti_{27}O_{24}(PO_4)_{24}$ based on a trimeric chromophore $[Cr^{III}Ti_2^{IV}O_{12}]$ (Fig. 4b) led to splittings of the second absorption band, which are in clear discrepancy with observation. The unreasonably low energy for the metal–ligand σ-interaction from this modelling is also a hint that the presence of $[Cr^{III}Ti_2^{IV}O_{12}]$ chromophores is rather unlikely. The low-lying charge-transfer is likely to be related to a transition from an oxide ion to titanium(IV).

4. Conclusions

The cation distribution, and therefore possible stable compositions, for anhydrous oxidephosphates of the lipscombite/lazulite structure family is determined by charge-balance considerations and (to a first approximation) by cation–cation repulsion. Full occupancy of all octahedral voids is possible only for rather small, not too highly charged cations (e.g. Ni^{II}/Cr^{III}) or in cases were metal–metal bonding can compensate to some extend for unfavourable electrostatic repulsion as is the case for $V^{II}V^{III}O(PO_4)$ and β-$Fe^{II}Fe^{III}O(PO_4)$. Average oxidation numbers higher than 2.5+ for the cations are only possible if a sufficient number of voids is created, that will allow relaxation of the (now even higher) electrostatic repulsion. In this respect, it becomes quite clear that any, even minute, oxidation of β-$Fe^{II}Fe^{III}O(PO_4)$ to $\square_x Fe^{II}_{1-3x}Fe^{III}_{1+2x}O(PO_4)$ will lead to the electrostatically very unfavourable distribution of five Fe^{3+} over six voids. Introducing tetravalent cations in the structure type gives immediately a higher number of voids per unit cell (lower occupancy in Fig. 10). Thus trimers $[M^{II}M_2^{IV}O_{12}]$ and the apparently very favourable distribution of dimers $[M^{III}M^{IV}O_9]$ and $[M_2^{IV}O_9]$ in addition to vacancies become possible. Moving to even higher average charges for the cations leads to even lower occupancies. This is realized in $\square_3Ti_5^{IV}O_4(PO_4)_4$ by the formation of "monomeric" $[Ti^{IV}O_6]$ units in addition to voids and dimers $[Ti_2^{IV}O_9]$. The composition $M_4^{III}Ti_{27}O_{24}(PO_4)_{24}$ (M = Ti, Cr, Fe), that appears on first sight rather strange, is just the result of the 1:1 combination of two quite stable cation distribution patterns and their related chemical compositions.

It is yet an open question to which extent an introduction of pentavalent or hexavalent cations (e.g. V^V, Nb^V, Mo^V, Mo^{VI}) into the lipscombite/lazulite structure together with an even lower occupancy of the octahedral voids will be tolerated.

Acknowledgments

We thank Dr. Jörg Daniels (Univ. of Bonn, Germany) and Mrs. Chun-Yu Chen (NTHU Hsinchu, Taiwan) for recording of the single-crystal data sets. We also thank Prof. Johannes Beck (Univ. of Bonn, Germany) and Prof. Sue-Lein Wang (NTHU Hsinchu, Taiwan) for the friendly provision of the instruments. M.S. thanks the DAAD for providing a scholarship. The great hospitality and stimulating scientific support by Prof. Sue-Lein Wang (NTHU Hsinchu, Taiwan), Prof. Kwang-Hwa Lii (NCU Chongli, Taiwan) and all their group members is gratefully acknowledged.

Appendix A. Supplementary data

Supplementary data associated with this article can be found in the online version at doi:10.1016/j.jssc.2008.02.039.

Reference

[1] M. Schöneborn, Part of Planned Ph.D. Thesis, University of Bonn.
[2] F. Reinauer, R. Glaum, R. Gruehn, Eur. J. Inorg. Solid State Chem. 31 (1994) 779.
[3] F. Reinauer, Ph.D. thesis, University of Gießen, 1998.
[4] F. Reinauer, R. Glaum, Acta Crystallogr. B 54 (1998) 722.
[5] L. Katz, W.N. Lipscomb, Acta Crystallogr. 4 (1951) 345.
[6] M.A. Gheith, Am. Miner. 38 (1953) 612.
[7] M. Ijaali, B. Malaman, C. Gleitzer, J.K. Warner, J.A. Hriljac, A.K. Cheetham, J. Solid State Chem. 86 (1990) 195.
[8] B. Ech-Chahed, F. Jeannot, B. Malaman, C. Gleitzer, J. Solid State Chem. 74 (1988) 47.
[9] E. Elkaim, J.F. Berar, C. Gleitzer, B. Malaman, M. Ijjaali, C. Lecomte, Acta Crystallogr. B 52 (1996) 428.
[10] M. Schöneborn, R. Glaum, Z. Anorg. Allg. Chem. 633 (2007) 2568.
[11] C.C. Torardi, W.M. Reiff, L. Takacs, J. Solid State Chem. 82 (1989) 203.
[12] J.T. Vaughey, W.T.A. Harrison, A.J. Jacobson, D.P. Goshorn, J.W. Johnson, Inorg. Chem. 33 (1994) 2481.
[13] M.L. Lindberg, C.L. Christ, Acta Crystallogr. 1959 (1959) 20.
[14] P. Graverau, J.P. Chaminade, B. Manoun, S. Krimi, A. El Jazouli, Powder Diff. 14 (1999) 10.
[15] S. Benmokhtar, A. El Jazouli, J.P. Chaminade, P. Graverau, A. Wattiaux, L. Fournes, J.C. Grenier, D. Waal, J. Solid State Chem. 179 (2006) 3709.
[16] S. Benmokhtar, H. Belmal, A. El Jazouli, J.P. Chaminade, P. Graverau, S. Pechev, J.C. Grenier, et al., J. Solid State Chem. 180 (2007) 772.
[17] P. Graverau, S. Benmokhtar, J.P. Chaminade, A. El Jazouli, E. Lebraud, D. Denux, Solid State Sci. 9 (3) (2007) 258.
[18] E. Benser, R. Glaum, T. Droß, H. Hibst, Chem. Mater. 19 (2007) 4341–4348.
[19] S.T. Norberg, G. Svensson, J. Albertsson, Acta Crystallogr. C 57 (2001) 225.
[20] Y.E. Gorbunova, S.A. Linde, Dokl. Akad. Nauk SSSR 245 (1979) 584.
[21] H.-J. Koo, M.-H. Whangbo, P.D. VerNooy, C.C. Torardi, W.J. Marshall, Inorg. Chem. 41 (2002) 4664.
[22] S. Geupel, K. Pilz, S. van Smaalen, F. Buellesfeld, A. Prokofiev, W. Assmus, Acta Crystallogr. C 58 (2002) i9.
[23] E.V. Murashova, N.N. Chudinova, Kristallografiya 39 (1) (1994) 145.
[24] V.V. Krasnikov, Z.A. Konstant, Izv. Akad. Nauk SSSR, Neorg. Mater. 15 (1979) 2164.
[25] S. Andersson, B. Collen, U. Kuylenstierna, A. Magneli, Acta Chem. Scand. 11 (1957) 1641.
[26] H. Horiuchi, N. Morimoto, M. Tokonami, J. Solid State Chem. 17 (1976) 407.
[27] H. Schäfer, Chemische Transportreaktionen, Verlag Chemie, Weinheim, 1962.
[28] R. Gruehn, R. Glaum, Angew. Chem. Int. Ed. 39 (2000) 692.
[29] A. Winkler, E. Thilo, Z. Anorg. Allg. Chem. 346 (1966) 92.
[30] G. Brauer, Handbuch der präparativen anorganischen Chemie, Ferdinand Enke Verlag, Stuttgart, 1975, 1508pp.
[31] Y. Ameniya, J. Miyahara, Nature (1998) 89.
[32] I. Tanaka, M. Yao, M. Suzuki, K. Hikichi, J. Appl. Crystallogr. 23 (1990) 334.
[33] K. Maaß, R. Glaum, R. Gruehn, Z. Anorg. Allg. Chem. 626 (2002) 1663.
[34] J. Soose, G. Meyer, SOS—Programme zur Auswertung von Guinier-Aufnahmen, Univ. of Gießen, 1980.
[35] E. Krausz, AOS News 12 (1998) 21.
[36] E. Krausz, Aust. J. Chem. 46 (1993) 1041.
[37] M. Voda, J. Garcia Sole, F. Jaque, I. Vergara, A. Kaminskii, B. Mill, A. Butashin, Phys. Rev. B49 (1994) 3755.
[38] U. Fano, Phys. Rev. 124 (1961) 1866.
[39] D. Neuhauser, T.J. Park, J.I. Zink, Phys. Rev. Lett. 85 (2000) 5304.
[40] L.J. Farrugia, J. Appl. Cryst. 32 (1999) 837.
[41] G.M. Sheldrick, XPREP 6.12, SHELXTL, Bruker-AXS, Madison, WI, USA.
[42] G.M. Sheldrick, Acta Crystallogr. A46 (1990) 467.
[43] G.M. Sheldrick, University of Goettingen, Germany, 1997.
[44] N. Middlemiss, C. Calvo, Acta Crystallogr. B 32 (1976) 2896.
[45] M. Gruß, R. Glaum, Acta Crystallogr. C 52 (1996) 2647.
[46] D.A. Cruse, J.E. Davies, J.H. Harding, M. Gerloch, D.J. Mackey, R.F. McMeeking, "CAMMAG," 1980, a FORTRAN program, Cambridge.
[47] M. Gerloch, Magnetism and Ligand Field Theory, Cambridge University Press, 1983.
[48] M. Riley, "*CAMMAG for PC*," V 4.0, University of Queensland, St. Lucia, Australia, 1997.
[49] C.K. Jørgensen, R. Pappalardo, H.H. Schmidtke, J. Chem. Phys. 39 (1963) 1422.
[50] D.E. Richardson, J. Chem. Ed. 70 (1993) 372.
[51] B.N. Figgis, M.A. Hitchman, Ligand Field Theory and Its Applications, Wiley-VCH, New York, 2000.
[52] H. Thauern, R. Glaum, Inorg. Chem. 46 (2007) 2057.
[53] R. Glaum, Neue Untersuchungen an wasserfreien Phosphaten der Übergangsmetalle (in German), Thesis of Habilitation, University of Gießen, 1999. URL: 〈http://bibd.uni-giessen.de/ghtm/1999/uni/h990001.htm〉.
[54] T. Dahmen, R. Gruehn, Z. Kristallogr. 204 (1993) 57.
[55] D. Reinen, Struct. Bond. 6 (1969) 30.
[56] D. Reinen, M. Atanasov, S.L. Lee, Coord. Chem. Rev. 175 (1998) 91.
[57] R.H. Blessing, Acta Crystallogr. A 51 (1995) 33.